

This is the peer reviewed version of the following article: Zhang, Y., Wu, Z., Li, P., Ono, L. K., Qi, Y., Zhou, J., Shen, H., Surya, C., Zheng, Z., Adv. Energy Mater. 2018, 8, 1701569, which has been published in final form at <https://doi.org/10.1002/aenm.201701569>. This article may be used for non-commercial purposes in accordance with Wiley Terms and Conditions for Use of Self-Archived Versions.

DOI: 10.1002/((please add manuscript number))

Article type: Communication

Fully Solution-processed TCO-free Semi-transparent Perovskite Solar Cells for Tandem and Flexible Applications

Yaokang Zhang¹, Zhongwei Wu¹, Peng Li¹, Luis K. Ono², Yabing Qi², Jixiang Zhou³, Hui Shen^{3,4}, Charles Surya⁴, Zijian Zheng^{1,}*

Mr. Yaokang Zhang, Dr. Zhongwei Wu, Mr. Peng Li, Prof. Zijian Zheng

1. Laboratory for Advanced Interfacial Materials and Devices, Institute of Textiles and Clothing, the Hong Kong Polytechnic University, Hong Kong, China

E-mail: tczzheng@polyu.edu.hk

Dr. Luis K. Ono, Prof. Yabing Qi

2. Energy Materials and Surface Sciences Unit (EMSS), Okinawa Institute of Science and Technology Graduate University (OIST), 1919-1 Tancha, Onna-son, Okinawa, 904-0497, Japan

Mr. Jixiang Zhou, Prof. Hui Shen

3. Institute for Solar Energy Systems, Sun Yat-Sen University, Guangzhou, Guangdong Province, P.R. China

Mr. Jixiang Zhou, Prof. Charles Surya

4. Department of Electronic and Information Engineering, the Hong Kong Polytechnic University, Hong Kong, China

Keywords: perovskite solar cells; TCO-free; solution process; semi-transparent solar cells; tandem solar cells

Abstract

Semi-transparent perovskite solar cells (st-PSCs) have received remarkable interest in recent years because their great potential in applications for solar window, tandem solar cells, and flexible photovoltaics. However, all reported st-PSCs require expensive transparent conducting oxides (TCOs) or metal-based thin films made by vacuum deposition, which is not cost effective for large scale fabrication: the cost of TCOs is estimated to occupy approximately 75% of the manufacturing cost of PSCs. To address this critical challenge, we report herein a low-temperature and vacuum-free strategy for the fabrication of highly efficient TCO-free st-PSCs. Our TCO-free st-PSC on glass exhibits 13.9% power conversion efficiency (PCE), and the four-terminal tandem cell made with our st-PSC top cell and c-Si bottom cell shows an overall PCE of 19.2%. Due to the low processing temperature, we also demonstrate the fabrication of flexible st-PSCs on polyethylene terephthalate (PET) and polyimide (PI), which show excellent stability under repeated bending or even crumbing.

Semi-transparent solar cells have drawn unprecedented attention for their appealing applications in recent years. The color and transmittance of the semi-transparent solar cells are adjustable through methods like optical engineering of the active absorbers^[1, 2] or the transparent electrodes^[3, 4], which fit a wide variety of applications ranging from solar glass for buildings and solar curtains for upholstery, to wearable electronics and fashion^[5, 6]. More importantly, these semi-transparent devices can stack on commercial Si solar cells to build a tandem structure, which will further improve the efficiency to harvest solar energy without increasing the area of the devices^[7-9].

Among the different kinds of absorbers suitable for making semi-transparent solar cells, organolead halide perovskites (typically $\text{CH}_3\text{NH}_3\text{PbI}_3$) have showed great advantage owing to their low cost, high charge-carrier mobility, high absorption coefficient, and good solution-processability^[10-21]. Groups of researchers have been intensively investigating better perovskite materials in the past decade. Recently, perovskite materials have demonstrated their capability of producing opaque solar cells with very high power conversion efficiency (PCE) over 20%, a milestone which can compete with Si-based solar technology^[22]. More importantly, the absorption spectrum of perovskite materials can be tuned to fit the complementary wavelength of the bottom Si device, so as to maximize the absorption of the solar energy in a tandem device^[23-26]. As such, it is very promising to fabricate highly efficient and bandgap tunable semi-transparent perovskite solar cells (st-PSCs).

From a device point of view, apart from the perovskite absorbers, another key challenge to build an efficient st-PSC is how to fabricate low-cost top and bottom transparent electrodes with high transmittance and high conductivity. Up till now, however, it is still necessary to use expensive vacuum deposition technique and materials to fabricate at least one of the electrodes of st-PSCs. For the bottom electrodes, most st-PSCs were built with indium tin oxide (ITO) or fluorine-doped tin oxide (FTO), which show high transmittance ($\sim 85\%$) and low sheet resistance ($\sim 15 \Omega/\text{sq}$)^[27]. However, the cost of these transparent conducting oxides (TCOs) is very high: the estimated cost of TCO electrodes accounts for $\sim 75\%$ of the total cost of a perovskite solar module^[28], which is not economically viable for large-scale application. Besides the cost issue, these TCOs are mechanically brittle and therefore their applications on future flexible and wearable types of devices are also largely restricted^[29, 30]. On the other hand, reported top transparent electrodes of st-PSCs include aluminum-doped zinc oxide (AZO)^[31], $\text{MoO}_3/\text{Au}/\text{MoO}_3$ ^[32], graphene^[33] and graphene-based electrodes^[21, 34, 35]. Unfortunately, the fabrication of these top electrodes either requires vacuum technology that is sizing-limiting or relies on multiple time-consuming etching process. To the best of our knowledge, there is no report on TCO-free st-PSCs that can be fabricated in a solution-processable manner, which is highly desirable for large-area and high-throughput roll-to-roll (R2R) manufactory^[36, 37].

To address the challenge, we report here a low-temperature and fully solution-processed approach to fabricating efficient TCO-free st-PSCs, which are applicable to tandem and flexible applications. In this approach, each functional layer in the PSCs is processed by a simple and fast solution-based casting or printing method. In particular, nitric acid annealed conducting polymer poly(3,4-ethylenedioxythiophene) polystyrene sulfonate (PEDOT:PSS) is used as both transparent cathode and anode of the device to replace TCO, while low temperature processed ZnO is used as the electron transporting layer (ETL) of the device. The champion TCO-free st-PSC on glass (TCO-free@glass) fabricated by this approach shows a remarkable efficiency of 13.9%. The st-PSC is readily integrated with Si solar cells to yield a four-terminal PSC/Si tandem solar cell, which exhibits an overall PCE of 19.2%. In addition, because the entire fabrication is processed with a temperature lower than 130 °C, we also demonstrate the fabrication of highly flexible and efficient TCO-free st-PSCs on polyethylene terephthalate (PET) and polyimide (PI) using this approach.

Among the many substitutes of TCOs, PEDOT:PSS is one of the most promising candidates because of its low cost and solution processability, which shows good compatibility with R2R processes^[38-40]. Previous studies have proved that acid treatment can significantly improve the conductivity of PEDOT:PSS^{[41], [42]}. In this study, we find that an acid-annealing with nitric acid provides the best conductivity, as well as making the PEDOT:PSS film printable. Therefore, fully solution-processed

electrodes are realized by replacing traditional TCO-based and/or metal based bottom and top electrodes with ~50 nm thick, highly conductive n-PEDOT:PSS (nitric acid annealed PEDOT:PSS) films. To avoid the decomposition of PEDOT:PSS, TiO₂ compact layer which typically requires high temperature annealing (~500 °C) is not used.^{39, 40} Instead, a low-temperature (130 °C) processed ZnO thin layer is applied as the ETL as well as hole blocking layer. 2,2',7,7'-tetrakis(N,N'-di-p-methoxyphenylamine)-9,9'-spirobifluorene (spiro-OMeTAD) is used as hole transporting layer (HTL) of the device. The band structure of the device is given in **Figure 1**. Importantly, the entire device fabrication is free from high vacuum or high temperature treatment.

As illustrated in Figure 1a, the solution fabrication of TCO-free st-PSCs started with the bottom transparent electrode on glass. PEDOT:PSS was spin-coated on cleaned sodium glass substrates, followed by a nitric acid annealing to yield the n-PEDOT:PSS bottom electrode. Subsequently, a ZnO precursor solution was spin-coated on n-PEDOT:PSS, followed by thermal annealing at 130 °C to remove the solvent and to form a dense nanocrystal layer. Then, the perovskite layer was deposited through a one-step method by spin-coating a mixed cation perovskite precursor solution and then annealing at 100 °C for 2 min. After the formation of the dark brown perovskite film, ~200 nm thick spiro-OMeTAD was deposited by spin-coating its chlorobenzene solution. Here, spiro-OMeTAD serves not only as hole HTL but also as a smoothening layer to reduce the surface roughness (Figure S1).

Such an interfacial layer is crucial for the successful transfer of n-PEDOT:PSS top electrode as introduced later on.

For the fabrication of top electrode, direct spin-coating of aqueous PEDOT:PSS on top of the spiro-OMeTAD will significantly degrade the device due to the high sensitivity of the perovskite layer to moisture^[43, 44]. Therefore, we fabricated the n-PEDOT:PSS firstly on a Si substrate and dry transfer-printed onto spiro-OMeTAD (Figure 1a). In brief, a flat polydimethylsiloxane (PDMS) stamp was placed on the n-PEDOT:PSS, which was fabricated on a cleaned Si substrate. Due to the weaker interaction with the Si surface and a stronger interaction with PDMS, n-PEDOT:PSS was easily peeled off from the Si substrate with the PDMS stamp. To ensure a strong and conformal contact between the n-PEDOT:PSS and spiro-OMeTAD, we applied a short air plasma treatment (~ 3s) of the n-PEDOT:PSS prior to the transfer and a short thermal treatment (2 min at ~60 °C) after the contact of the these two surfaces. The transfer process was finished by lifting up the PDMS stamp and leaving the n-PEDOT:PSS top electrode on spiro-OMeTAD. The SEM cross-sectional image indicates an intimate contact between the spiro-OMeTAD layer and the top n-PEDOT:PSS electrode (Figure 1b). Detailed information for the fabrication process is provided in the Methods section.

To investigate whether n-PEDOT:PSS is suitable for transparent electrode application, the surface morphology, optical transmittance, sheet resistance and work function of

the thin film were studied in detail. Pristine PEDOT:PSS (p-PEDOT:PSS) and sulfuric acid-annealed PEDOT:PSS (s-PEDOT:PSS) films were also studied as reference. The preparation of p-PEDOT:PSS and s-PEDOT:PSS are provided in the Methods section.

In order to form high quality ETL and active layers, the bottom transparent electrode is required to be uniform and smooth. The thickness of the p-PEDOT:PSS was 170 nm. After the acid treatment, the thickness decreased dramatically to 50 nm (**Figure 2a**). The root mean square roughness (R_q) of n-PEDOT:PSS was ~ 1.5 nm, which was similar to that of p-PEDOT:PSS and s-PEDOT:PSS, according to the atomic force microscopy (AFM) analysis. Such a smooth thin film ensures the subsequent fabrication of devices, which can also be evidenced by the cross-sectional SEM image shown in Fig 1b. All the PEDOT:PSS films showed $>80\%$ transmittance at 550 nm, which is comparable to that of ITO (Figure 2b). It should be noted that the optical transmittance of the treated PEDOT:PSS are slightly lower than p-PEDOT:PSS, which indicates a stronger conjugation of the PEDOT:PSS after acid treatment. Indeed, the acid treatment decreases significantly the sheet resistance. While p-PEDOT:PSS showed a very large sheet resistance of ~ 1 M Ω /sq, the sheet resistance of s-PEDOT:PSS and n-PEDOT:PSS were remarkably reduced to 50 Ω /sq and 38 Ω /sq, respectively. As shown in Figure 2c, the work function of the electrode also decreased significantly after the acid treatment. Through ultraviolet photoelectron spectroscopy (UPS) measurement, both s-PEDOT:PSS and n-PEDOT:PSS samples showed a similar work function of ~ 4.2 eV, which is ~ 0.4 eV lower than that of p-PEDOT:PSS. This

value is similar to polycrystalline Ag fabricated by thermal evaporation, which is often used as electrode of different kinds of photovoltaic devices.

In order to understand the mechanism of acid treatment, we carried out X-ray photoelectron spectroscopy (XPS) and Raman spectroscopy to analyze the thin film composition. It should be noted that the decrease in film thickness, sheet resistance, and work function indicates strongly the removal of PSS through acid treatment. Therefore, we focused the analysis on the PSS content. There are two types of S atoms in PEDOT:PSS (**Figure 3 a, b**). One is from the thiophenic S in PEDOT (binding energy 163~166 eV), while the other arises from the sulfonate S in PSS (binding energy 167~171 eV). The PSS component in pristine PEDOT:PSS consisted of 1:2 molar ratio of PSS^-H^+ and PSS^-Na^+ , among which the Na^+ originates from the oxidizing process during the polymerization of PEDOT. From the XPS analysis, the PEDOT to PSS ratio of p-PEDOT:PSS was determined to be 0.94. After acid treatment, a dramatic decrease in the S and O peaks of PSS component was found and the PEDOT to PSS ratio of s-PEDOT:PSS and n-PEDOT:PSS increased to 4.4 and 4.9, respectively. In addition, there's no peak among the XPS core level region of N 1s (**Figure 3c**), which indicates that the nitric acid treatment did not cause N-doping or impurity to PEDOT:PSS. Raman spectroscopy is consistent with what we have observed from the XPS analysis. After acid treatment, the peak intensity at 1263 cm^{-1} , 1365 cm^{-1} , 1427 cm^{-1} and 1508 cm^{-1} increased significantly, indicating a larger proportion of PEDOT component (**Figure 3d**). Note that the Raman spectrum of

s-PEDOT:PSS is almost identical to that of p-PEDOT:PSS, and there is no peak shift of the strong stretching mode signal at 1427 cm^{-1} . These evidences indicate that the acid treatment cause no oxidation on the thiophenic rings of PEDOT, but a structural change from benzoid to quinoid which appeared with formic acid treatment^[45].

From the XPS and Raman analysis, we can conclude that the acid treatment partially removed the PSS from the thin films, but was not strong enough to oxidize them. Therefore, it leads to thinner film thickness, lower sheet resistance, and decreased work function. Nitric acid treatment removed more PSS than sulfonic acid treatment^[42, 46]. Therefore, it is reasonable that n-PEDOT:PSS possesses a lower sheet resistance. For transparent electrode application, the higher conductivity and transmittance of n-PEDOT:PSS makes it a better candidate comparing with s-PEDOT:PSS.

In our device fabrication, low-temperature processed ZnO is used as ETL to replace TiO₂, which often requires high temperature annealing. However, the basic nature of ZnO may lead to the degradation of perovskite during thermal annealing^[47], which is an inevitable step to evaporate the solvent and to turn the perovskite layer to a “black” phase. Therefore, the optimum annealing time of perovskite layer was studied first. To eliminate the possible influence of new electrode materials, we used a standard opaque reference device (opaque ref.) with a structure of ITO/ZnO/Perovskite/spiro-OMeTAD/Au for this study. As illustrated in **Figure 4a**, 2

min annealing at 100 °C of the perovskite layer resulted in satisfactory device performance, yielding a V_{OC} of 1.06 V, J_{SC} of 23.1 mA/cm², FF of 74%, and a PCE of 18.1%. Longer annealing time lead to a dramatic decrease of solar cell efficiency. For example, when the annealing time was extended to 10 min, only 7.7% PCE was obtained. The photovoltaic effect almost extinguished as the annealing time went up to 30 min. Since 2 min annealing was necessary to ensure the good formation of perovskite layer, we determined 2 min as a standard annealing time for all other device fabrication in the following sections.

Secondly, we studied the suitability of transfer-printed n-PEDOT:PSS as top electrode of st-PSCs. Reference semi-transparent devices with a device structure of ITO/ZnO/Perovskite/spiro-OMeTAD/n-PEDOT:PSS (ITO ref.) were fabricated for this study. The ITO ref. device showed a V_{OC} of 1.14 V, a J_{SC} of 21.5 mA/cm², and an FF of 67%, resulting in a PCE of 16.4% when illuminated from the bottom side (ITO side). To the best of our knowledge, this value is the highest among all the reported st-PSCs in the literature (Table S1). When illuminated from the n-PEDOT:PSS side, the ITO ref. device showed a slight decrease in J_{SC} to 18.2 mA/cm², resulting in a PCE of 14.2%. These results confirm that the transfer-printed top n-PEDOT:PSS is suitable for making st-PSCs. The detailed parameters of the st-PSCs are summarized in Table 1.

We then replaced the ITO bottom electrode with our n-PEDOT:PSS electrode to study the fully solution-processed TCO-free st-PSCs. Remarkably, the TCO-free@glass showed a V_{OC} of 1.06 V, a J_{SC} of 19.3 mA/cm², and an FF of 68%, resulting in a PCE of 13.9% when illuminated from the bottom side. Similar to the ITO ref. device, when the device was illuminated from the top side, the PCE showed a small decrease to 12.6%. Considering that previously reported TCO-free perovskite solar cells showed very limited PCE values, our result is extraordinary even when compared with those opaque TCO-free devices based on highly conductive metal electrodes.

To further understand the change in J_{SC} in different device configurations and testing conditions, external quantum efficiency (EQE) of the ITO ref. and TCO-free@glass were measured (Figure 4c). When illuminated from the bottom side, the EQE of both types of devices reached a maximum value at wavelength of ~500 nm. The integral J_{SC} of TCO-free@glass is 17.3 mA/cm² according to the EQE spectrum. This result is slightly (~10%) lower than that observed from J - V curve (19.3 mA/cm²), which is probably due to the mismatch between the spectrum of EQE and I - V testing systems. The EQE of TCO-free@glass showed a higher slope after the peak absorption, which is due to the lower transmittance of n-PEDOT:PSS at longer wavelength. The EQE results explain the lower current density of TCO-free@glass that was observed in the J - V characterization. It should also be noted that an obvious drop from 400 to 450 nm in EQE spectra was observed when illuminating the device from the top side. This can be ascribed to the strong light absorption of spiro-OMeTAD at UV (Figure S2). Such

difference in transmittance explains the lower output current density of the device when illuminated from the top side.

One appealing application of st-PSCs is the integration with monocrystalline Si solar cell (c-Si) to form tandem devices. As such, one can obtain much higher energy harvesting without occupying more area for the placing the device. For our solution-processed TCO-free device, the use of low-cost materials and fabrication is particularly attractive for this application. As a proof-of-concept, we fabricated a four-terminal st-PSC/c-Si tandem solar cell using TCO-free@glass as the top cell and c-Si as the bottom cell (**Figure 5a**). The average optical transmittance of the TCO-free@glass is 42.0%, and most of the transmittance occurs at wavelengths >800 nm (**Figure 5b**). The remarkable transmittance of our st-PSCs at near-infrared region is critical for high performance tandem cells based on c-Si bottom cells. The J-V characteristics of the cells are shown in **Figure 5c**, and the detailed parameters are listed in **Table 2**. The c-Si solar cell adopted an anti-reflection design with pyramidal surface texture and Si₃N₄ coating to make full use of the transmitted light through the top perovskite solar cell. Such an anti-reflection treatment resulted in a large short-circuit current density of 39.3 mA/cm² and high external quantum efficiency for the standalone c-Si solar cell (**Figure S3**). The c-Si cell we fabricated showed an efficiency of 17.4%. Combined with the 13.9% TCO-free@glass, the filtered c-Si cell exhibited a PCE of 5.3%, thus the overall efficiency of the four-terminal tandem devices was 19.2%. From EQE analysis (**Figure 5d**), we observed that while the

TCO-free@glass top cell converted near-UV and visible light (300 ~ 800 nm) to electricity, approximately half of the photocurrent of c-Si solar cell was raised from the absorption of near infrared light (800 ~ 1200 nm).

Because of the low-temperature processing ability and the use of PEDOT:PSS electrodes, our TCO-free st-PSC is also very suitable for use in flexible applications.

As proof-of-concept, we fabricated flexible TCO-free st-PSCs on 125 μm thick PET (TCO-free@PET). Since the nitric acid treatment can cause damage to PET, the bottom PEDOT:PSS electrode was prepared by transfer printing n-PEDOT:PSS onto PET. The rest of the fabrication steps remained the same as those for making TCO-free st-PSC on glass. The J-V curves in **Figure 6a** and **b** were measured during top illuminating of the devices. TCO-free@PET showed a V_{OC} of 0.99 V, a J_{SC} of 17.3 mA/cm^2 , an FF of 60%, and a PCE of 10.3%. Compared with TCO-free st-PSC on rigid glass substrate, the lower PCE is mainly due to the decrease in J_{SC} and FF , which is probably due to the higher surface roughness and defects of PET. TCO-free@PET is highly bendable. We tested the flexibility of TCO-free@PET device by repeating bending of the device at a radius of 5 mm. Over 90% of the initial PCE was maintained after 1,000 cycles of bending. The ~10% drop in PCE majorly is a result of the decrease in J_{SC} . Interestingly, we also observed an obvious increased in FF after the bending test. Comparing with other reported flexible PSCs^[48-50], our TCO-free@PET showed the best retention under bending tests. When using an ultrathin plastic substrate, the flexibility of the device can even be improved much further. Figure 6d showed a crumbled TCO-free st-PSC fabricated on 1 μm thick PI

(TCO-free@PI), which possessed a V_{OC} of 0.99 V, a J_{SC} of 14.2 mA/cm², an FF of 55%, and a PCE of 7.7%. The device is highly conformable to arbitrary curved surface due to its ultrahigh flexibility (Figure 6d).

We have reported the first low-temperature and solution fabrication of TCO-free st-PSCs. The key to achieve the device fabrication is the utilization of highly conductive n-PEDOT:PSS as both bottom and top transparent electrodes. Our TCO-free st-PSC fabricated on glass showed a PCE of 13.9 %, which is the most efficient solution-processed perovskite devices reported to date. The TCO-free st-PSC could readily stack c-Si bottom cell to build a four-terminal st-PSC/c-Si tandem cell, which showed an overall PCE of 19.2%. Note that the new fabrication approach is entirely vacuum-free and is conducted under a low temperature, which is ideal for making flexible devices. Indeed, our flexible st-PSC fabricated on PET substrate exhibited 10.3 % efficiency and maintained >90% of this initial value after 1,000 cycles of bending at a small radius of 5 mm. We believe that our results are significant for realizing R2R fabrication of high performance and low-cost PSCs, which is promising for large area tandem solar cells and flexible electronics in the future.

Experimental Section

Materials and synthesis: Patterned ITO/glass slides were purchased from Zhuhai Kaivo Optoelectronic Technology Co., Ltd.) Polydimethylsiloxane (PDMS) prepolymer and the curing agent (Sylgard 184) were purchased from Dow Corning.

The two reagents were mixed at a ratio of 10:1 (w/w), degassed and cured at 70 °C for about 2 h to prepare cross-linked PDMS stamp. PbI₂ (99.999%), PbBr₂ (99.999%), formamidinium iodide (FAI, >98%), methylammonium bromide (MABr, 98%), bis(trifluoromethane)sulfonimide lithium salt (Li-TFSI, 99.95%), and 4-tert-butylpyridine (tBP, 96%) were purchased from Sigma-aldrich. 2,2',7,7'-tetrakis(N,N-di-p-methoxyphenylamine)-9,9'-spirobifluorene (Spiro-OMeTAD, 99.5%) was purchased from Derthon Optoelectronic Materials Science Technology Co., Ltd. Highly conductive PEDOT:PSS solution (Clevios PH 1000, 1.0 ~ 1.3 wt.% in water) was purchased from Heraeus. The ZnO precursor was prepared by a simple hydrolysis method reported elsewhere. Briefly, 1 g zinc acetate dehydrate was dissolved in a mixture of 275 µL ethanolamine and 10 mL 2-methoxyethanol. The solution was kept in ambient environment under strong stirring for 12 h. The perovskite precursor solution consists of 2.645 g PbI₂, 0.372 g PbBr₂, 0.940 g FAI, 0.113 g MABr, 4 mL dimethylformamide (DMF), and 1 mL dimethyl sulfoxide (DMSO). The solution was ready for use after stirring for 30 min at room temperature. All these solutions were filtered by 0.45 µm PTFE filter before use.

Substrate preparation: For TCO-free devices, PET films and glass substrates were cut to 2 cm × 2 cm size. Then the films or slides were cleaned by ultrasonication in acetone, isopropanol and deionized (DI) water bath for 30 min, respectively. Glass slides were cleaned with piranha solution (H₂SO₄ : H₂O₂ = 3:1) for 10 min to remove

the organic residues and to improve the wettability. For PI films, the precursor solution (poly(pyromellitic dianhydride-co-4,4'-oxydianiline), amic acid solution, 15.0 wt.% \pm 5 wt.% in NMP/aromatic hydrocarbons (80%/20% solvent ratio), Sigma-Aldrich) was spin-coated on glass slides at 4000 rpm for 1 min, then the sample was heated at 200 °C in vacuum oven for 2 h. PET and PI films were treated with plasma for 5 min before use.

p-PEDOT:PSS, s-PEDOT:PSS and n-PEDOT:PSS for Characterization:
p-PEDOT:PSS, s-PEDOT:PSS and n-PEDOT:PSS films were prepared on glass for the characterization of optical transmittance, UPS, XPS and Raman spectroscopy. Firstly, PEDOT:PSS solution was spin-coated on cleaned glass substrates 500 rpm for 5 s and 1000 rpm for 1 min, followed by 125 °C annealing for 10 min. For s-PEDOT:PSS or n-PEDOT:PSS, the samples were then immersed in 95% H₂SO₄, or 70% HNO₃, respectively. After 10 min acid annealing, the samples were rinsed by DI water, and then annealed at 120 °C for 10 min to removal residual water.

Solar cells on glass: For ITO ref. device, ITO/glass was cleaned by ultrasonic bath of acetone, isopropanol and DI water for 30 min each. The ITO slide was then treated with plasma to improve the wettability. ZnO precursor solution was spin-coated at 4000 rpm for 1min. The ZnO layer was then annealed at 130 °C for 30 min. For TCO-free@glass, nitric acid-annealed PEDOT:PSS was used as bottom electrode instead of ITO. A glass slide was firstly treated by piranha solution (H₂SO₄:H₂O = 3:1,

volume ratio) for 10 min and then rinsed with DI water. Then PEDOT:PSS solution was spin-coated on the glass slide at 500 rpm for 5 s and 1000 rpm for 1 min, followed by 125 °C annealing for 10 min. The PEDOT:PSS film was then immersed in 70% nitric acid bath for 10 min. Afterwards the slide was rinsed and dried on a hot plate at 120 °C. A diluted ZnO precursor solution (volume ratio 1:1 with isopropanol) was spin-coated on PEDOT:PSS film at 5000 rpm for 30s and then annealed at 130 °C for 5 min to serve as compact layer before the spin-coating of the ZnO precursor solution. The sample was then transferred to a N₂-filled glovebox, and 40 µL perovskite precursor solution^[51] was spin-coated on ZnO at 6000 rpm for 30 s. 150 µL chlorobenzene was dropped atop the spinning slides at 20 s of the spin-coating step. After coating of the perovskite layer, the sample was annealed at 100 °C for 30 min. Then, 40 µL spiro-OMeTAD solution was spin-coated atop the perovskite layer at 5000 rpm for 20 s. The solution contains 70 mg spiro-OMeTAD, 25 µL Li-TFSI solution (520 mg/mL in acetonitrile), and 36 µL *t*BP in 1 mL chlorobenzene. Finally, n-PEDOT:PSS film was transfer-printed atop the spiro-OMeTAD layer. For the opaque reference device, 100 nm of Au was deposited on the spiro-OMeTAD layer at 0.3 nm/s by thermal evaporation. Au bars were also deposited along one edge of both bottom and top n-PEDOT:PSS electrodes to improve the contact between the electrodes and testing wires.

Flexible St-PSCs: For st-PSC@PET, n-PEDOT:PSS was transfer-printed on PET as bottom electrode. For st-PSC@PI, the n-PEDOT:PSS electrode was directly

fabricated on PI using the acid treatment process. The acid treatment was performed by dropping 50 μL nitric acid on the slide rather than dipping the slide in nitric acid, because dipping would exfoliate the PI film from the glass slide. The rest part of the fabrication on flexible substrates was same as the procedures on rigid glass substrate. For the ultrathin TCO-free@PI devices, the PI substrates were peeled-off from the glass slides after the device fabrication was finished.

c-Si solar cells: Boron-doped Cz-mono-Si wafers were used as the bulk of c-Si solar cells. The cutting damage of Si wafers was eliminated by immersing in 20% wt. KOH solution at 80 °C. Random pyramid texture of the Si wafers for light trapping was achieved by immersing in a mixed solution of 5% wt. KOH, isopropanol and additives at 80 °C. After etching the SiO_2 by HF solution, the wafers were loaded into a diffusion furnace with POCl_3 gas where the p-n junction formed at the diffusion temperature of 830 °C for 20 min. The entire surface of the wafers was covered by a phosphorus-doped layer ($\sim 70 \text{ } \Omega/\text{sq}$). The back junction was etched by a mixed solution of $\text{HF}:\text{HNO}_3:\text{H}_2\text{O}$ (1:5:4). The upper surface of the Si solar cells was passivated by $\sim 80 \text{ nm}$ of $\text{SiN}_x:\text{H}$ deposited by plasma-enhanced chemical vapor deposition (PECVD). $\text{Al}_2\text{O}_3/\text{SiN}_x:\text{H}$ double layer passivation was adopted for the back surface of Si wafers. After opening a certain pattern on $\text{Al}_2\text{O}_3/\text{SiN}_x:\text{H}$ by laser to expose part of the back surface, uniform Al paste and Ag paste were printed on the back and top surface of Si wafers by screen printing technology, respectively. Al paste and Ag paste were co-fired at peak temperature of 780 °C, when the Ag paste etched

the SiN_x:H top surface and contacted the Si.

Four-terminal tandem cell: The four-terminal tandem cell was fabricated by placing TCO-free@glass st-PSC atop c-Si solar cell. The effective area of the st-PSC was slightly large than that of c-Si bottom cell to ensure that the bottom cell was covered completely. Then the solar cells were fixed and encapsulated by epoxy glue. Ag pastes and Cu tapes were used to improve the contact between electrodes and testing wires for J - V and EQE measurement.

Characterizations: The optical transmittance was measured by Agilent Cary 7000 UV-Vis spectrometer. The AFM topographic images were obtained with an XE-100 AFM (Park Systems, Suwon, South Korea) in non-contact mode. The ITO reference, pristine and treated PEDOT:PSS were characterized by ultraviolet photoemission spectroscopy (Kratos AXIS ULTRA HAS, He-I α = 21.22 eV) and X-ray photoelectron spectroscopy (XPS, Kratos AXIS ULTRA HAS, monochromated Al K α = 1486.6 eV). The SEM images were measured by a CARL ZEISS ULTRA 55 scanning electron microscope. The J - V characteristics of the devices were characterized by a Keithley 2400 sourcemeter. To simulate standard sunlight, a solar simulator with AM 1.5 filter (91160, Newport, 100 mW/cm²) was used as the light source. The solar simulator was calibrated by a standard Si solar cell before use. To determine the active area of the device, a shadow mask (0.11 cm²) was attach on the device before testing. The EQE of the devices were measured with a standard system consists of a xenon lamp (Oriel

66902, 300 W), a monochromator (Newport 66902), a Si detector (Oriel 76175_71580) and a dual channel power meter (Newport 2931_C).

Supporting Information

Supporting Information is available from the Wiley Online Library or from the author.

Acknowledgements

We acknowledge the financial support from The Hong Kong Polytechnic University (Project 1-ZVK1) and the Guangdong-Hong Kong Technology Cooperation Funding Scheme (2014B050505010). L.K.O. and Y.B.Q. would like to acknowledge funding from the Energy Materials and Surface Sciences Unit of the Okinawa Institute of Science and Technology Graduate University, the OIST R&D Cluster Research Program, the OIST Proof of Concept (POC) Program and JSPS KAKENHI Grant Number 15K17925.

References

- [1] C.-C. Chen, L. Dou, J. Gao, W.-H. Chang, G. Li, Y. Yang, *Energy Environ. Sci.* **2013**, 6, 2714.
- [2] R. E. Beal, D. J. Slotcavage, T. Leijtens, A. R. Bowring, R. A. Belisle, W. H. Nguyen, G. F. Burkhard, E. T. Hoke, M. D. McGehee, *J. Phys. Chem. Lett.* **2016**, 7, 746.
- [3] Y. H. Chen, C. W. Chen, Z. Y. Huang, W. C. Lin, L. Y. Lin, F. Lin, K. T. Wong, H. W. Lin, *Adv. Mater.* **2014**, 26, 1129.
- [4] Y. Jiang, B. Luo, F. Jiang, F. Jiang, C. Fuentes-Hernandez, T. Liu, L. Mao, S. Xiong, Z. Li, T. Wang, *Nano Lett.* **2016**, 16, 7829.
- [5] J. Huang, G. Li, Y. Yang, *Adv. Mater.* **2008**, 20, 415.
- [6] T. Miyazaki, A. Akisawa, T. Kashiwagi, *Renew. Energy* **2005**, 30, 281.
- [7] J. Y. Kim, K. Lee, N. E. Coates, D. Moses, T.-Q. Nguyen, M. Dante, A. J. Heeger, *Science* **2007**, 317, 222.
- [8] J. You, L. Dou, K. Yoshimura, T. Kato, K. Ohya, T. Moriarty, K. Emery, C.-C. Chen, J. Gao, G. Li, *Nat. Comm.* **2013**, 4, 1446.
- [9] C. C. Chen, W. H. Chang, K. Yoshimura, K. Ohya, J. You, J. Gao, Z. Hong, Y. Yang, *Adv. Mater.* **2014**, 26, 5670.
- [10] N.-G. Park, *J. Phys. Chem. Lett.* **2013**, 4, 2423.
- [11] C. Wehrenfennig, G. E. Eperon, M. B. Johnston, H. J. Snaith, L. M. Herz, *Adv. Mater.* **2014**, 26, 1584.
- [12] C. S. Ponseca Jr, T. J. Savenije, M. Abdellah, K. Zheng, A. Yartsev, T. r. Pascher, T. Harlang, P. Chabera, T. Pullerits, A. Stepanov, *J. Am. Chem. Soc.* **2014**, 136, 5189.
- [13] S. D. Stranks, G. E. Eperon, G. Grancini, C. Menelaou, M. J. Alcocer, T. Leijtens, L. M. Herz, A. Petrozza, H. J. Snaith, *Science* **2013**, 342, 341.
- [14] H. J. Snaith, *J. Phys. Chem. Lett.* **2013**, 4, 3623.
- [15] J. You, Z. Hong, Y. M. Yang, Q. Chen, M. Cai, T. B. Song, C. C. Chen, S. Lu, Y. Liu, H. Zhou, Y. Yang, *ACS Nano* **2014**, 8, 1674.
- [16] D. Yang, R. Yang, J. Zhang, Z. Yang, S. F. Liu, C. Li, *Energy Environ. Sci.* **2015**.
- [17] D. Liu, T. L. Kelly, *Nat. Photon.* **2014**, 8, 133.
- [18] M. Kaltenbrunner, G. Adam, E. D. Głowacki, M. Drack, R. Schwödiauer, L. Leonat, D. H. Apaydin, H. Groiss, M. C. Scharber, M. S. White, *Nat. Mater.* **2015**, 14, 1032.
- [19] G. E. Eperon, V. M. Burlakov, A. Goriely, H. J. Snaith, *ACS nano* **2013**, 8, 591.
- [20] Z. Li, S. A. Kulkarni, P. P. Boix, E. Shi, A. Cao, K. Fu, S. K. Batabyal, J. Zhang, Q. Xiong, L. H. Wong, *ACS nano* **2014**, 8, 6797.
- [21] P. You, Z. Liu, Q. Tai, S. Liu, F. Yan, *Adv. Mater.* **2015**.
- [22] N. J. Jeon, J. H. Noh, W. S. Yang, Y. C. Kim, S. Ryu, J. Seo, S. I. Seok, *Nature* **2015**, 517, 476.
- [23] C. D. Bailie, M. G. Christoforo, J. P. Mailoa, A. R. Bowring, E. L. Unger, W. H. Nguyen, J. Burschka, N. Pellet, J. Z. Lee, M. Grätzel, *Energy Environ. Sci.* **2015**, 8, 956.
- [24] D. P. McMeekin, G. Sadoughi, W. Rehman, G. E. Eperon, M. Saliba, M. T.

- Hörantner, A. Haghighirad, N. Sakai, L. Korte, B. Rech, *Science* **2016**, 351, 151.
- [25] S. Albrecht, M. Saliba, J. P. C. Baena, F. Lang, L. Kegelmann, M. Mews, L. Steier, A. Abate, J. Rappich, L. Korte, *Energy Environ. Sci.* **2016**, 9, 81.
- [26] J. H. Heo, S. H. Im, *Adv. Mater.* **2015**.
- [27] C. J. Emmott, A. Urbina, J. Nelson, *Sol. Energy Mater. Sol. Cells* **2012**, 97, 14.
- [28] M. Cai, Y. Wu, H. Chen, X. Yang, Y. Qiang, L. Han, *Adv. Sci.* **2016**.
- [29] S. K. Hau, H.-L. Yip, J. Zou, A. K.-Y. Jen, *Org. Electron.* **2009**, 10, 1401.
- [30] J. F. Salinas, H. L. Yip, C. C. Chueh, C. Z. Li, J. L. Maldonado, A. K. Y. Jen, *Adv. Mater.* **2012**, 24, 6362.
- [31] F. Fu, T. Feurer, T. P. Weiss, S. Pisoni, E. Avancini, C. Andres, S. Buecheler, A. N. Tiwari, *Nat. Energy* **2016**, 2, 16190.
- [32] F. Zhou, Z. Ren, Y. Zhao, X. Shen, A. Wang, Y. Y. Li, C. Surya, Y. Chai, *ACS nano* **2016**, 10, 5900.
- [33] F. Lang, M. A. Gluba, S. Albrecht, J. R. Rappich, L. Korte, B. Rech, N. H. Nickel, *J. Phys. Chem. Lett.* **2015**, 6, 2745.
- [34] Y. Li, L. Meng, Y. M. Yang, G. Xu, Z. Hong, Q. Chen, J. You, G. Li, Y. Yang, Y. Li, *Nat. Comm.* **2016**, 7.
- [35] M. Dianetti, F. Di Giacomo, G. Polino, C. Ciceroni, A. Liscio, A. D'Epifanio, S. Licoccia, T. Brown, A. Di Carlo, F. Brunetti, *Sol. Energy Mater. Sol. Cells* **2015**, 140, 150.
- [36] F. C. Krebs, T. Tromholt, M. Jørgensen, *Nanoscale* **2010**, 2, 873.
- [37] K. Hwang, Y. S. Jung, Y. J. Heo, F. H. Scholes, S. E. Watkins, J. Subbiah, D. J. Jones, D. Y. Kim, D. Vak, *Adv. Mater.* **2015**, 27, 1241.
- [38] F. C. Krebs, S. A. Gevorgyan, J. Alstrup, *J. Mater. Chem.* **2009**, 19, 5442.
- [39] D. Angmo, T. T. Larsen - Olsen, M. Jørgensen, R. R. Søndergaard, F. C. Krebs, *Adv. Energy Mater.* **2013**, 3, 172.
- [40] H. Sirringhaus, T. Kawase, R. Friend, T. Shimoda, M. Inbasekaran, W. Wu, E. Woo, *Science* **2000**, 290, 2123.
- [41] C. Yeon, S. J. Yun, J. Kim, J. W. Lim, *Adv. Electron. Mater.* **2015**, 1.
- [42] N. Kim, H. Kang, J. H. Lee, S. Kee, S. H. Lee, K. Lee, *Adv. Mater.* **2015**, 27, 2317.
- [43] T. Leijtens, G. E. Eperon, N. K. Noel, S. N. Habisreutinger, A. Petrozza, H. J. Snaith, *Adv. Energy Mater.* **2015**.
- [44] J. You, L. Meng, T.-B. Song, T.-F. Guo, Y. M. Yang, W.-H. Chang, Z. Hong, H. Chen, H. Zhou, Q. Chen, *Nat. Nanotech.* **2015**.
- [45] J. E. McCarthy, C. A. Hanley, L. J. Brennan, V. G. Lambertini, Y. K. Gun'ko, *J. Mater. Chem. C* **2014**, 2, 764.
- [46] Y. Xia, K. Sun, J. Ouyang, *Adv. Mater.* **2012**, 24, 2436.
- [47] Y. Han, S. Meyer, Y. Dkhissi, K. Weber, J. M. Pringle, U. Bach, L. Spiccia, Y.-B. Cheng, *J. Mater. Chem. A* **2015**, 3, 8139.
- [48] B. J. Kim, D. H. Kim, Y.-Y. Lee, H.-W. Shin, G. S. Han, J. S. Hong, K. Mahmood, T. K. Ahn, Y.-C. Joo, K. S. Hong, *Energy Environ. Sci.* **2015**, 8, 916.
- [49] H. Zhang, J. Cheng, F. Lin, H. He, J. Mao, K. S. Wong, A. K.-Y. Jen, W. C. Choy, *ACS nano* **2015**, 10, 1503.

- [50]X. Wang, Z. Li, W. Xu, S. A. Kulkarni, S. K. Batabyal, S. Zhang, A. Cao, L. H. Wong, *Nano Energy* **2015**, *11*, 728.
- [51]Y. H. Lee, J. Luo, M. K. Son, P. Gao, K. T. Cho, J. Seo, S. M. Zakeeruddin, M. Grätzel, M. K. Nazeeruddin, *Adv. Mater.* **2016**.

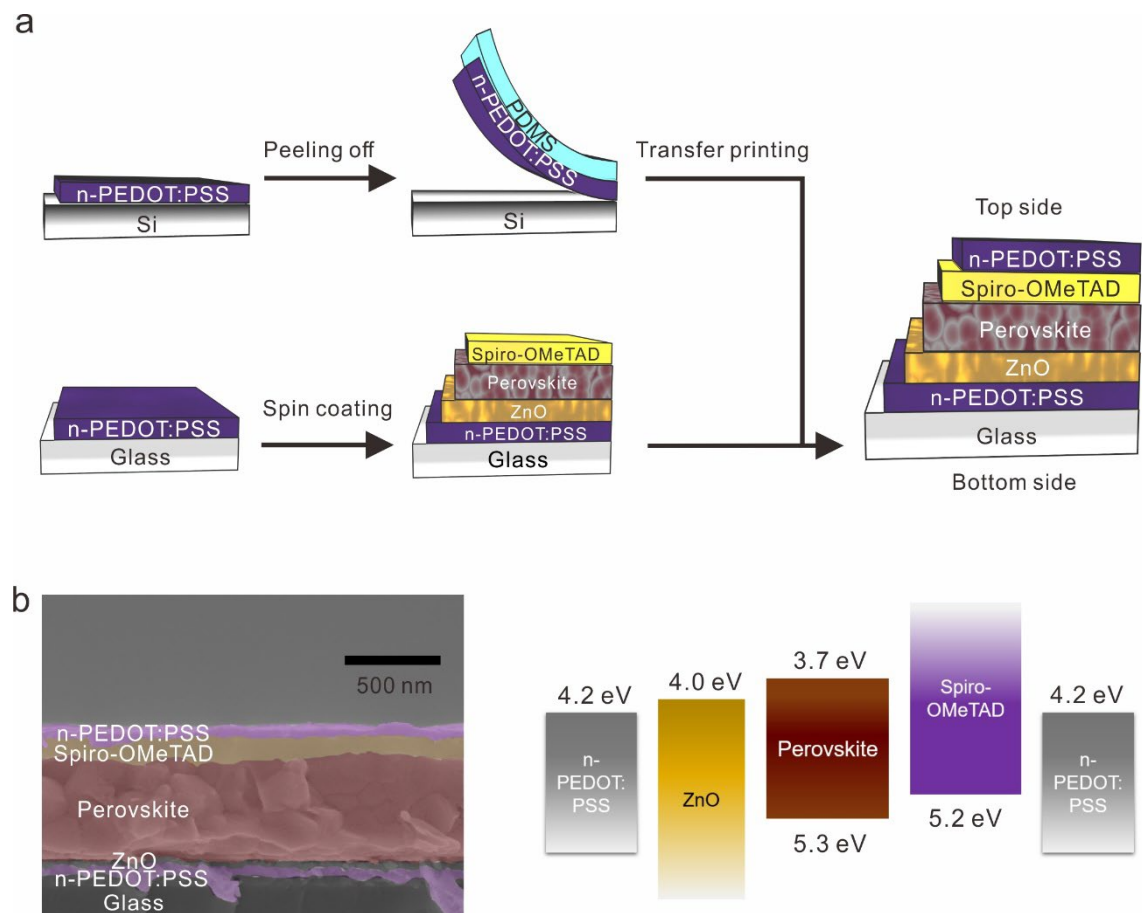


Figure 1. a) The schematic illustration of the fabrication process. b) SEM cross-sectional image (left) and energy-level diagram (right) of the TCO-free st-PSC. Scale bar is 500 nm.

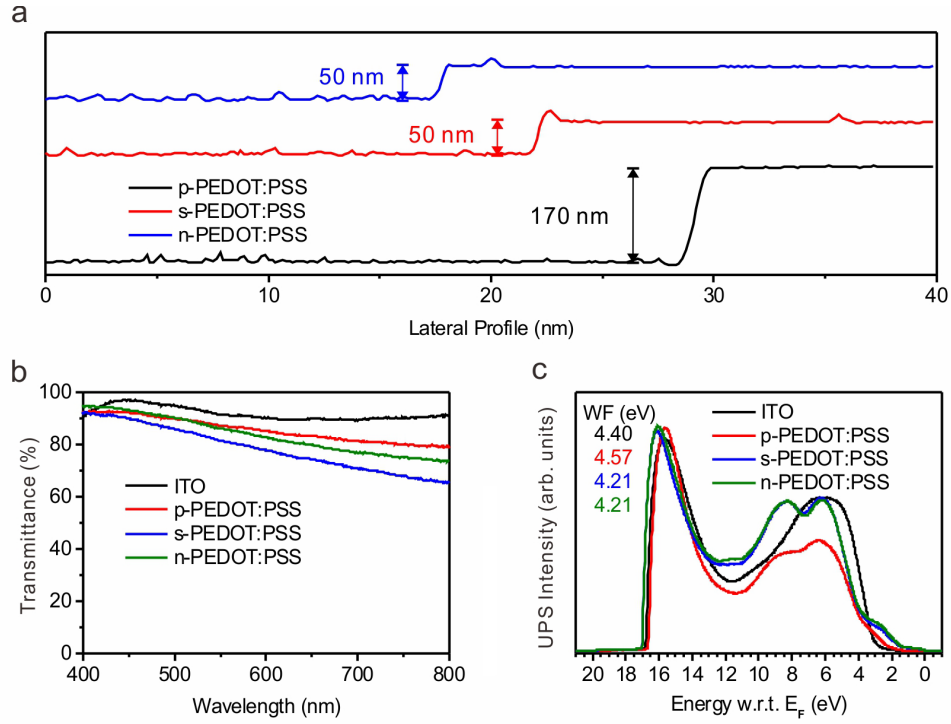


Figure 2. a) AFM profiles of the scratched edge of the p-PEDOT:PSS, s-PEDOT:PSS, and n-PEDOT:PSS. b) UV-Vis spectra of ITO, p-PEDOT:PSS, s-PEDOT:PSS and n-PEDOT:PSS. c) UPS spectra (He-I α = 21.22 eV) showing the secondary electron onset (left side) and valance state region (right side) of ITO, p-PEDOT:PSS, s-PEDOT:PSS and n-PEDOT:PSS.

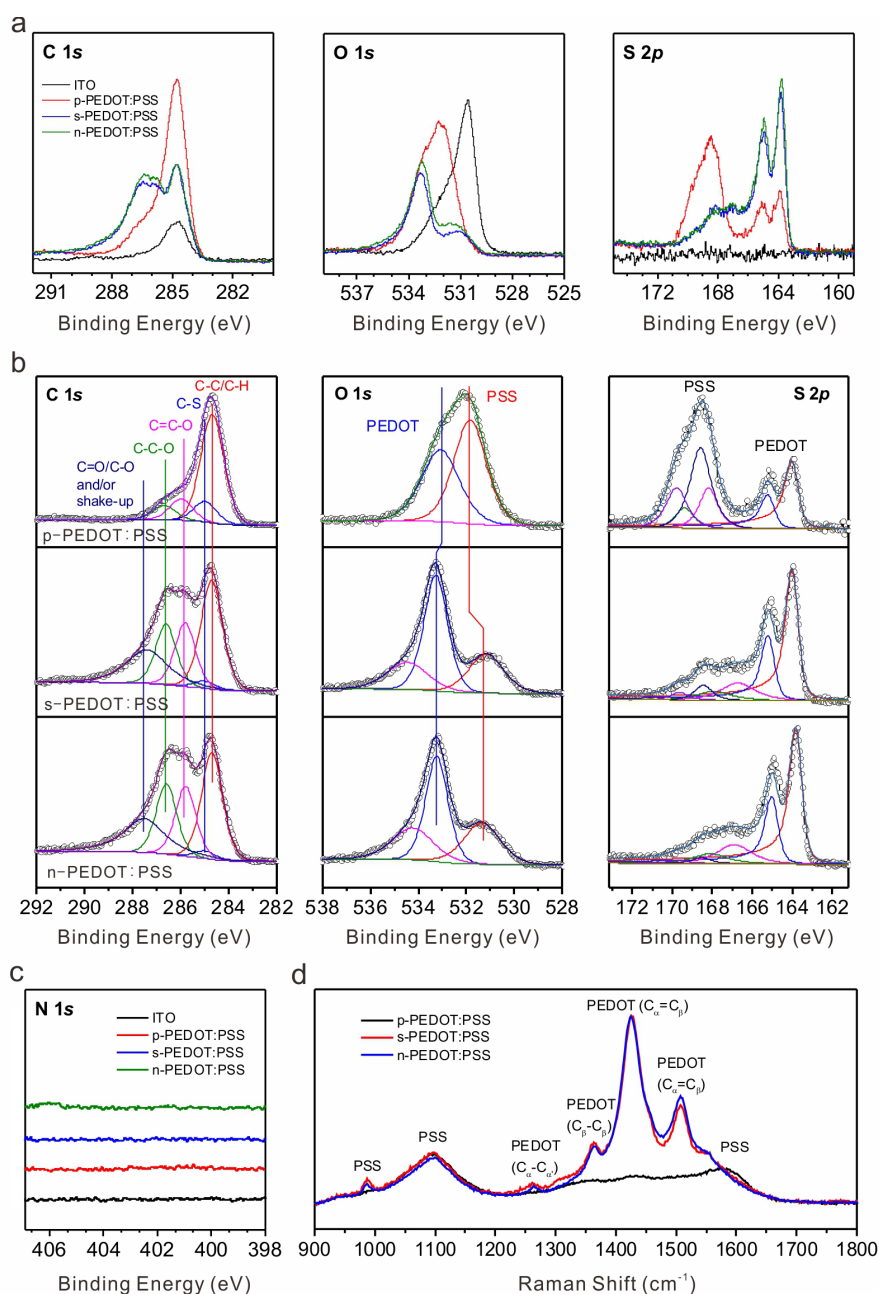


Figure 3. a) XPS spectra (Al-K α = 1253.6 eV) of the C 1s, O 1s and S 2p core levels of the ITO, p-PEDOT:PSS, s-PEDOT:PSS and n-PEDOT:PSS. b) Fitted XPS spectra corresponding to the C 1s, O 1s and S 2p core levels of the p-PEDOT:PSS, s-PEDOT:PSS and n-PEDOT:PSS. c) XPS N 1s core level of ITO, p-PEDOT:PSS, s-PEDOT:PSS and n-PEDOT:PSS. d) Raman spectra of p-PEDOT:PSS, s-PEDOT:PSS and n-PEDOT:PSS.

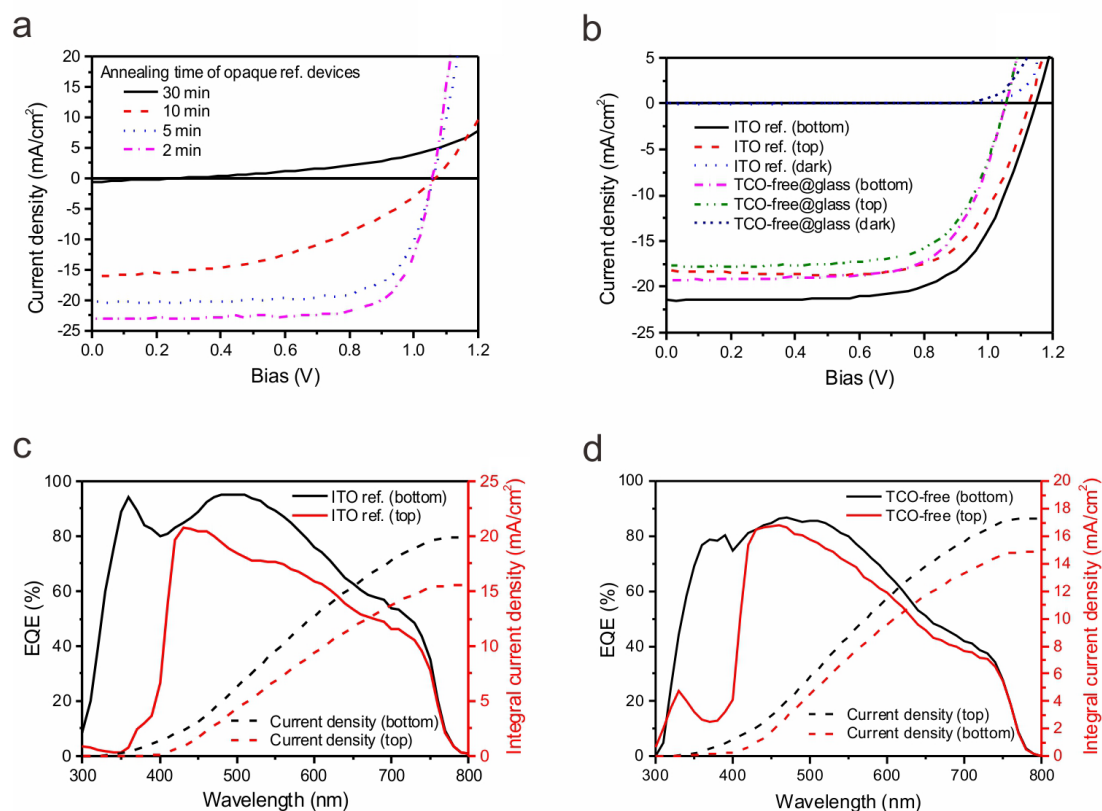


Figure 4. a) J-V curves of opaque ref. devices (ITO/ZnO/Perovskite/spiro-OMeTAD/Au) with different annealing time of perovskite layer. b) J-V curves of st-PSCs fabricated with n-PEDOT:PSS top electrode (ITO ref.) and n-PEDOT:PSS top and bottom electrodes (TCO-free@glass). c) and d) EQE spectra (solid lines) and integral current density (dash lines) of ITO based and TCO-free st-PSCs.

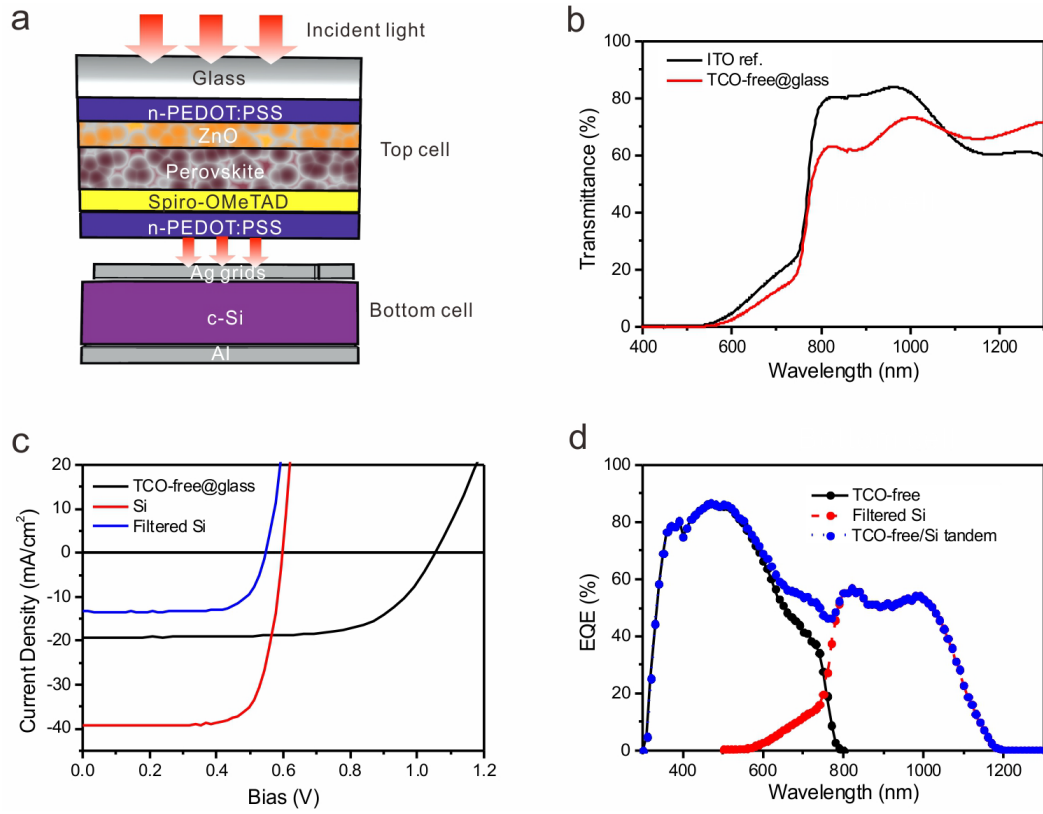


Figure 5. a) Illustration of the structure of the four-terminal TCO-free/c-Si tandem cell. b) Transmittance of ITO ref and TCO-free@glass cells. c) J-V curves of TCO-free@glass top cell and c-Si solar bottom cell as four-terminal tandem cell. d) EQE spectra of TCO-free@glass top cell and filtered c-Si bottom cell.

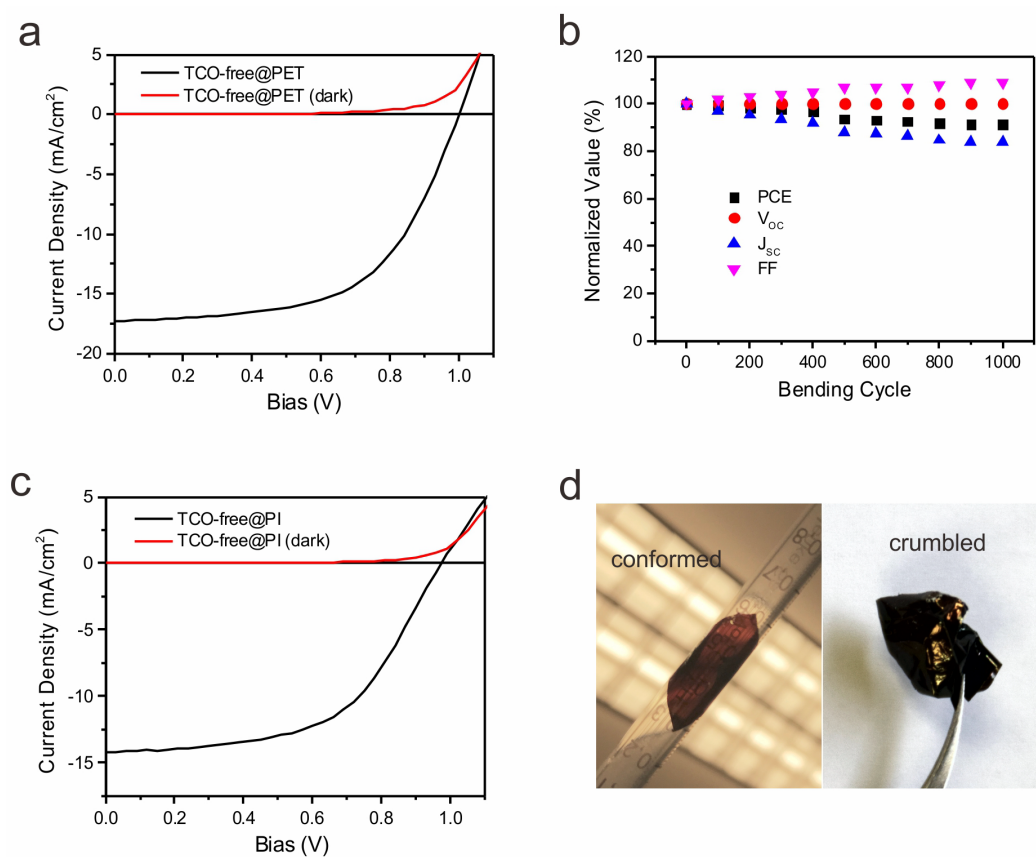


Figure 6. a) J-V curves of TCO-free@PET. b) Normalized photovoltaic characteristics of TCO-free@PET during 1000 bending at a radius of 5 mm. c) J-V curves of TCO-free@PI. d) Photographs of ultrathin TCO-free@PI conformably attached on a 1 mL syringe (left), and crumbled by a tweezer (right).

Table 1. Summary of photovoltaic characteristics of PSCs fabricated on glass.

Device type	V_{oc} (V)	J_{sc} (mA/cm²)	FF (%)	PCE (%)
ITO ref. (bottom illumination)	1.14	21.5	67	16.4
ITO ref. (top illumination)	1.13	18.2	69	14.2
TCO-free (bottom illumination)	1.06	19.3	68	13.9
TCO-free (top illumination)	1.06	17.8	67	12.6
Opaque ref.	1.06	23.1	74	18.1

Table 2. Summary of device performance of four-terminal tandem solar cells and flexible st-PSCs.

Device type	V_{oc} (V)	J_{sc} (mA/cm ²)	FF (%)	PCE (%)
TCO-free	1.06	19.3	68	13.9
c-Si	0.59	39.3	75	17.4
Filtered c-Si	0.54	13.2	75	5.3
TCO-free/c-Si Tandem				19.2
TCO-free@PET	0.99	17.3	60	10.3
TCO-free@PI	0.99	14.2	55	7.73

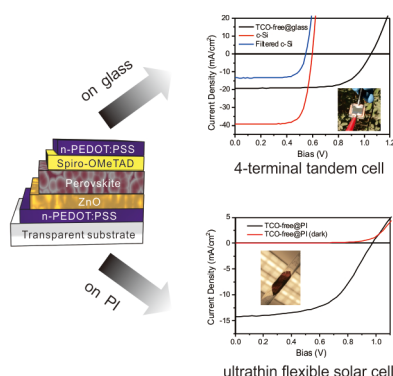
Fully solution-processed semi-transparent perovskite solar cells is reported for the first time to allow low-cost fabrication of highly efficiency tandem solar cells and flexible solar cells. Nitric acid annealed poly(3,4-ethylenedioxythiophene) polystyrene sulfonate is incorporated in the fabrication process to realize high-throughput printing of highly conductive transparent electrodes. The entire fabrication process is under low temperature, which is compatible with flexible polymeric substrates such as polyethylene terephthalate and polyimide.

Keyword:

perovskite solar cells; TCO-free; solution process; semi-transparent solar cells; tandem solar cells

Yaokang Zhang, Zhongwei Wu, Peng Li, Luis K. Ono, Yabing Qi, Jixiang Zhou, Hui Shen, Charles Surya, Zijian Zheng*

Fully Solution-processed TCO-free Semi-transparent Perovskite Solar Cells for Tandem and Flexible Applications



Supporting Information

Fully Solution-processed TCO-free Semi-transparent Perovskite Solar Cells for Tandem and Flexible Applications

*Yaokang Zhang¹, Zhongwei Wu¹, Peng Li¹, Luis K. Ono², Yabing Qi², Jixiang Zhou³,
Hui Shen^{3,4}, Charles Surya⁴, Zijian Zheng^{1,*}*

Mr. Yaokang Zhang, Dr. Zhongwei Wu, Mr. Peng Li, Prof. Zijian Zheng

1. Laboratory for Advanced Interfacial Materials and Devices, Institute of Textiles and Clothing, the Hong Kong Polytechnic University, Hong Kong, China

E-mail: tczzheng@polyu.edu.hk

Dr. Luis K. Ono, Prof. Yabing Qi

2. Energy Materials and Surface Sciences Unit (EMSS), Okinawa Institute of Science and Technology Graduate University (OIST), 1919-1 Tancha, Onna-son, Okinawa, 904-0497, Japan

Mr. Jixiang Zhou, Prof. Hui Shen

3. Institute for Solar Energy Systems, Sun Yat-Sen University, Guangzhou, Guangdong Province, P.R. China

Mr. Jixiang Zhou, Prof. Charles Surya

4. Department of Electronic and Information Engineering, the Hong Kong Polytechnic University, Hong Kong, China

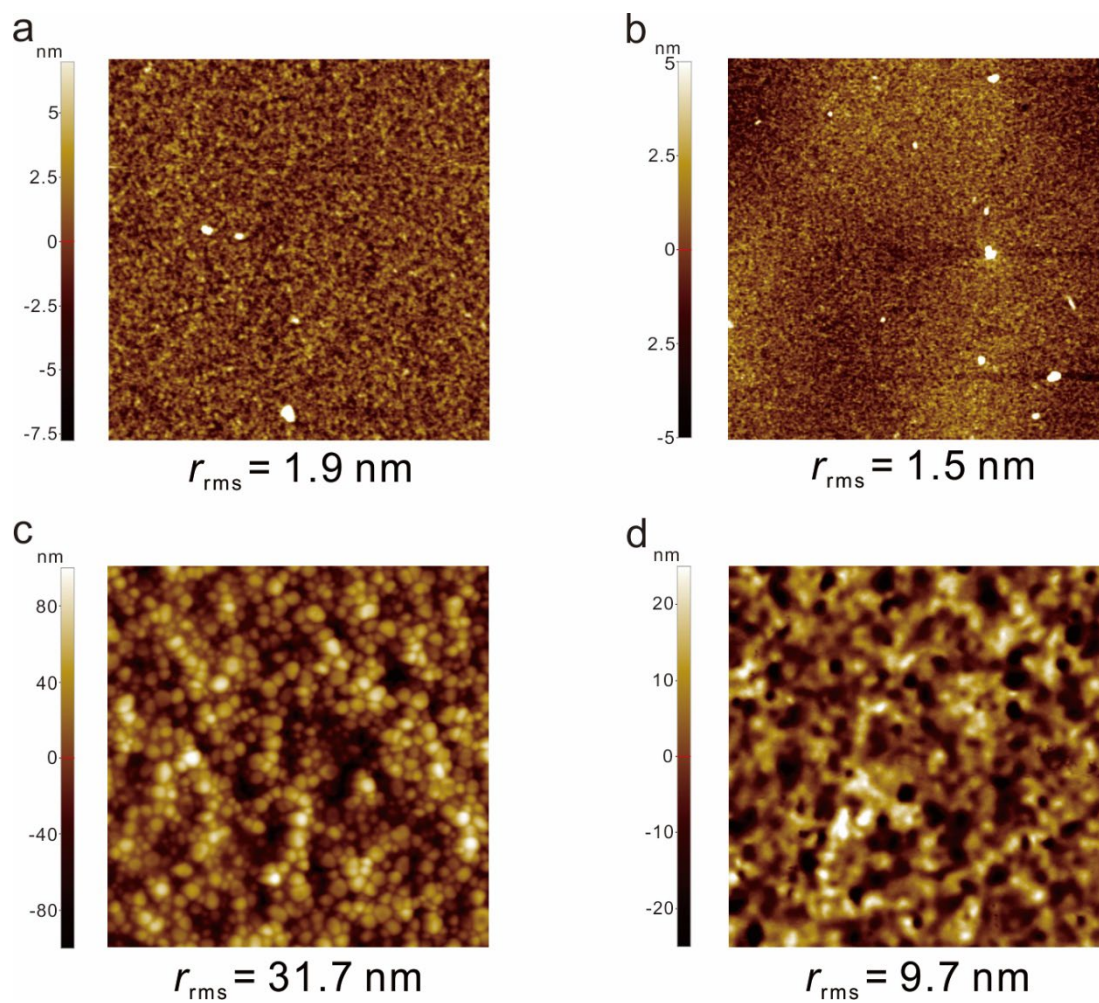


Figure S1. AFM topographic images of (a) n-PEDOT:PSS bottom electrode, (b) ZnO ETL, (c) perovskite active layer, and (d) spiro-OMeTAD HTL. Scan area is $10 \times 10 \text{ }\mu\text{m}$.

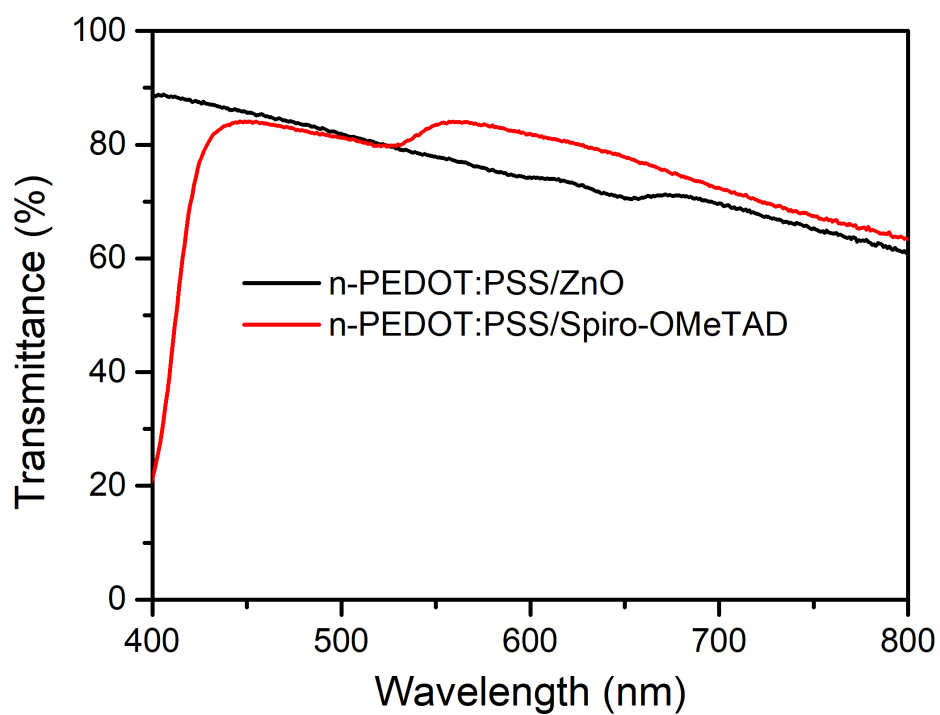


Figure S2. Optical transmittance of n-PEDOT:PSS/ZnO and n-PEDOT:PSS/Spiro-OMeTAD bilayer. Both samples were made on glass substrates.

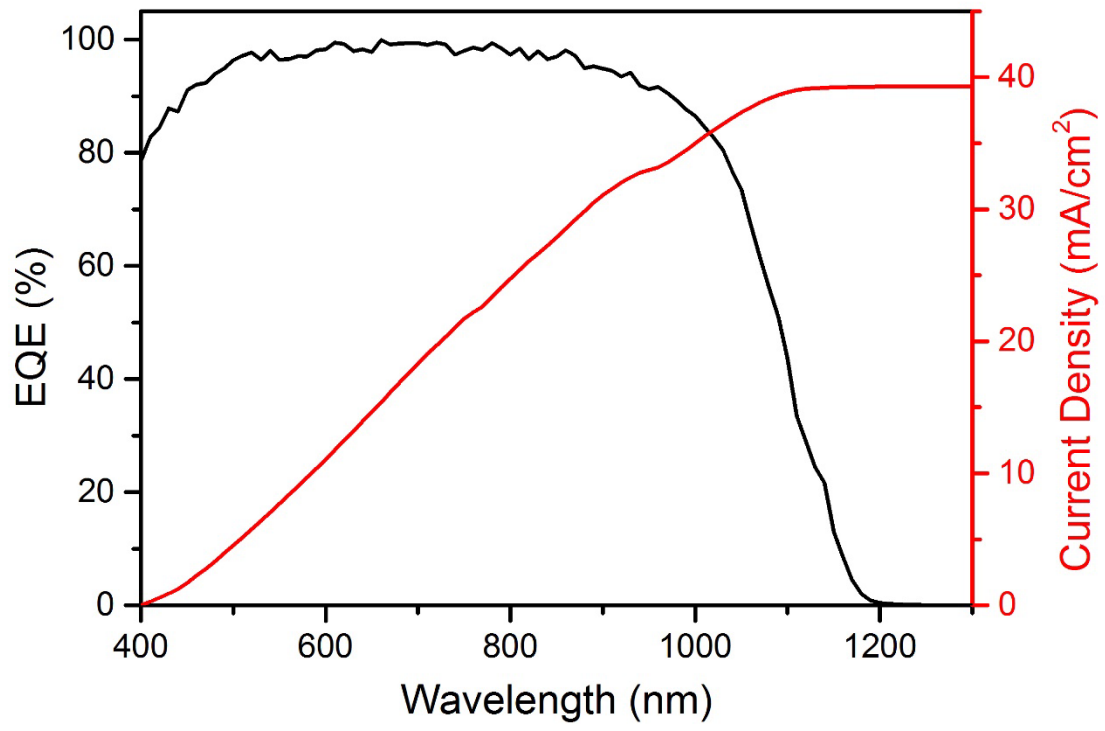


Figure S3. EQE spectrum and integrated short-circuit current density of standalone c-Si solar cell.

Table S1. Summary of state-of-the-art st-PSCs reported in the literature and by us

top//bottom electrodes	T _{max} (°C)	TCO -free	Vacuum -free	V _{OC} (V)	J _{sc} (mA/cm ²)	FF (%)	PCE (%)	active area (cm ²)	Source
FTO//AgNW	450	×	√	1.025	17.5	71	12.7	0.39	Energy & Environmental Science 8, 956-963 (2015)
FTO//ITO	185	×	×	1.1	19.9	70.7	15.1	/	Science 351, 151-155 (2016)
FTO//graphene	500	×	×	0.960	19.17	67.22	12.37	0.24	Advanced Materials 27, 3632-3638 (2015)
ITO//ITO	120	×	×	0.97	20.3	79	15.7	0.20	Science 354, 861-865 (2016)
ITO//ITO	350	×	×	1.08	16.69	75	13.52	0.10	Advanced Materials 28, 8990-8997 (2016)
ITO//AZO	200	×	×	1.116	19.1	75.4	16.1	0.29	Nature Energy 2, 16190 (2016)
ITO//PEDOT:PSS	130	×	√	1.14	21.5	67	16.4	0.11	This work
PEDOT:PSS//PEDOT:PSS	130	√	√	1.06	19.3	68	13.9	0.11	